Journal of Power Sources 216 (2012) 192–200

Contents lists available at SciVerse ScienceDirect

Journal of Power Sources

journal homepage: www.elsevier.com/locate/jpowsour

# An improved high-power battery with increased thermal operating range: C–$LiFePO_4$//C–$Li_4Ti_5O_{12}$

K. Zaghib [a,*], M. Dontigny [a], A. Guerfi [a], J. Trottier [a], J. Hamel-Paquet [a], V. Gariepy [a,b,c], K. Galoutov [a], P. Hovington [a], A. Mauger [b], H. Groult [c], C.M. Julien [c]

[a] Institut de Recherche d'Hydro-Québec, 1800 Lionel-Boulet, Varennes, Quebec, Canada J3X 1S1
[b] Institut de Minéralogie et de Physique des Milieux Condensés (IMPMC), Université Pierre et Marie Curie (UPMC), 4 place Jussieu, 75252 Paris Cedex 05, France
[c] Université Pierre et Marie Curie Paris-6, Laboratoire de Physicochimie des Electrolytes, Colloïdes et Sciences Analytiques (PECSA), UMR7195, 4 place Jussieu, 75005 Paris, France

## HIGHLIGHTS

- The 18650 cell was charged at 60C (1 min) with 80% of rated capability.
- $Li_4Ti_5O_{12}$ allows the replacement of $LiPF_6$ salt by LiTFSI and LiFSI in free EC for lower temperature.
- C–LTO depress the gas during charge discharge cycling and make technology very safe.

## ARTICLE INFO

*Article history:*
Received 19 March 2012
Received in revised form
8 May 2012
Accepted 11 May 2012
Available online 30 May 2012

*Keywords:*
Li-ion battery
Electrode performance
Thermal behavior
Electrolyte stability

## ABSTRACT

The carbon-coated $LiFePO_4$ and C–$Li_4Ti_5O_{12}$ particles of 90 nm in diameter have been tested as active elements of electrodes of Li-ion batteries. The 18650-size cell using the usual electrolyte 1 mol $L^{-1}$ $LiPF_6$ in ethylene carbonate (EC) and diethylene carbonate (DEC) displays a charge capacity of 650 mAh at low C-rate and retains more than 80% of rated capacity at 60C charge rate (1 min). 2032-size coin cells have been tested with different electrolytes: 1.5 mol $L^{-1}$ lithium tetrafluoroborate $LiBF_4$ in EC+ γ-butyrolactone (GBL), and 0.5 mol $L^{-1}$ lithium bis(trifluoromethanesulfonyl)imide ($LiN(CF_3SO_2)_2$, LiTFSI) + 1 mol $L^{-1}$ $LiBF_4$ in EC + GBL, aiming to replace the less stable $LiPF_6$ salt. The LiTFSI-based electrolyte can be used owing to the low operating voltage that avoids the corrosion of the aluminum of the collector. This electrolyte shows the best results as the performance is even higher at 60 °C. The infrared images show that the temperature of the cell never reaches this temperature during cycling, making this battery a high-power battery with remarkable thermal stability. The maximum temperature reached by the cell is 34 °C at 40C-rate and 40 °C at 60C. The free EC-based electrolytes even operate at 80 °C by using 1 mol $L^{-1}$ lithium bis(fluorosulfonyl)imide (LiFSI) in GBL or 1 mol $L^{-1}$ LiFSI in PC + GBL, thus increasing importantly the operating temperature range for the battery. The carbon coated on LTO depresses the evolution of gases during charge discharge.



## 1. Introduction

Intensive studies have been devoted to electrode materials for Li-ion batteries since they have supplemented Ni–MH batteries for demanding applications such as electric transportation hybrid (HEV) or electric (EV) vehicles. The battery is commonly identified by the name of the cathode element, because it is not only the most expensive part of the battery, but also the part that limits the electrochemical performance. After it has been recognized that $LiCoO_2$ is inappropriate for cost and safety reasons, $LiMn_2O_4$ spinel has been considered for a while as an alternative electrode [1,2]. At contrast to $LiCoO_2$ and more generally to the lamellar compounds of this family, $LiMn_2O_4$ has a good thermal stability. However, the manganese dissolves in the electrolyte. To solve this problem, manufacturers add to $LiMn_2O_4$ a lamellar compound that traps the manganese, but also re-introduces a material that lacks safety. The safety of the vehicles equipped with such a battery relies on a sophisticated battery monitoring system (BMS) that is costly, and is also the source of breakdowns. More recently, $LiFePO_4$ (LFP) has emerged as the solution to these problems. First proposed by Prof. Goodenough [3], this material shows a remarkable thermal stability. The intrinsic electronic conductivity is poor, but the coating of the particles with a conductive material, usually carbon, has solved this problem [4]. Nowadays, C–$LiFePO_4$ can be prepared

* Corresponding author. Tel.: +1 450 652 8019; fax: +1 450652 8424.
*E-mail address:* zaghib.karim@ireq.ca (K. Zaghib).

0378-7753/$ – see front matter © 2012 Elsevier B.V. All rights reserved.
doi:10.1016/j.jpowsour.2012.05.025

free of impurities, well crystallized, with a capacity close to its theoretical value 170 mAh $g^{-1}$ at an industrial scale, provided the quality control has been achieved [5].

Usually, the anode of the commercialized Li-ion batteries is in graphite, which has a good capacity and low $Li^+$/Li redox potential. On another hand, the anode element must afford safely fast charge and discharge. Regarding this property, $Li_4Ti_5O_{12}$ (LTO) has an advantage. The lack of strain in this material improves the shelf life. In contrast, the graphite suffers dilatation/contraction upon insertion/extraction of lithium, which results in aging, and limits the power of the battery. The theoretical capacity of $Li_4Ti_5O_{12}$ is 175 mAh $g^{-1}$. It is small compared to other anodes, but not prohibitive since it is slightly larger than that of $LiFePO_4$, and actually, the cathode's capacity limits that of the whole battery. The discharge voltage of $Li_4Ti_5O_{12}$ is close to 1.55 V *vs.* $Li^+$/Li, against 0.1 V for graphite. On one hand, it reduces the overall voltage of the battery and its energy density.

Replacement of carbon with lithium titanate anodes will lower the gravimetric and volumetric energy density of the resulting cell. There will be further reductions in energy density when utilizing high-power cell designs from 120 Wh $kg^{-1}$ for a C//LFP cell to 58 Wh $kg^{-1}$ for an LTO//LFP cell (calculated by weight of anode material). On the other hand, the fact that the voltage is higher than 1.0 V implies that $Li_4Ti_5O_{12}$ does not need passivation (no formation of the cell), at contrast to graphite and the other anode materials that inevitably react with the electrolyte. $Li_4Ti_5O_{12}$ is also preferred under high rate charge conditions compared to carbon since there will not be the likelihood of lithium plating occurring. That is why a lot of efforts were made already in the 90th's to optimize the preparation of $Li_4Ti_5O_{12}$ [6–15]. However, the power performance is limited by its low electronic conductivity. To overcome this problem, extensive works have been devoted to form nanoparticles [16–19], or to dope the material with metal cations [20–25], or to modify the surface [26,27], or to coat the particles with carbon [17,28–31] like those of $LiFePO_4$.

In a previous work, we have reported the properties of an LFP/LTO cell that passed successfully the battery tests for safety use in public transportation [32]. The "18650" battery prepared under such conditions delivers a capacity of 800 mAh. It retains full capacity after 20,000 cycles performed at charge rate 10C (6 min), discharge rate 5C (12 min), and retains 95% capacity after 30,000 cycles at charge rate 15C (4 min) and discharge rate 5C, both at 100% depth of discharge (DOD) and 100% state of charge (SOC). A demonstrator of this battery was presented at the World Energy council on an electric car, providing it with autonomy of 50 km. This is considered as too short for an EV, but it may be well suited to equip plug-in HEV's for instance. In this earlier work, the LFP particles were carbon coated but not the LTO, which was the limiting factor in terms of power.

The first goal of the present work is to investigate the LFP//LTO cell in which both the LFP and LTO particles have been carbon coated. As a result, this new cell still retains 50% of its capacity at 40C-rate, and does not age upon cycling, at least over the 3500 cycles that have been tested. Note the power of the battery increases upon decreasing the size of the particles, because the diffusion path inside the particles is reduced. In the present case, the average size of the particles is 90 nm. Since the size of the particles can be decreased down to about 20 nm [33], we believe that even more power will be accessed for the LFP//LTO batteries. For HEV and EV applications, however, such powers are useless, because it is not possible for the grid operators to supply consumers with so much power that a battery can be charged in 1 min 30 s, which corresponds to 40C rate. On another hand, we believe such batteries can find applications for smart grid projects, as they can be used to regulate the distribution of electricity.

Since the LFP//LTO batteries do not age upon cycling, their shelf life is limited only by the stability of the components, that of the electrolyte in particular. Power applications require an electrolyte with high ionic conductivity $\sigma > 10^{-3}$ S $cm^{-1}$ [34], a condition that is fulfilled by the most commonly used blend that consists of ethylene carbonate (EC) and diethyl carbonate (DEC) (EC:DEC, 1:1 by volume), the Li salt being $LiPF_6$. We report hereunder the tests of the cell with this electrolyte. However, the $LiPF_6$ is known to degrade. It decomposes at temperatures as low as 80 °C in the presence of organic solvents; the products of this decomposition induce acid (HF) dissolution of cathode active materials [35,36]. The organic solvents are also a problem. They can dissolve (decompose) the solid electrolyte interface (SEI) [37,38], and generate direct reactions between cathode active materials and the electrolyte [39]. The consequence is the fast deterioration of the batteries above 60 °C, and in practice the reason why the electric cars are equipped with a cooling system that keeps the temperature of the Li-ion batteries below 30 °C. The second goal of the present work is then to explore other lithium salts and other electrolytes that would not have this inconvenience. We present in this work the results obtained with two other electrolytes: 1.5 mol $L^{-1}$ lithium tetrafluoroborate $LiBF_4$ in EC + γ-butyrolactone (GBL) (1:1 by volume), and 0.5 mol $L^{-1}$ lithium bis(trifluoromethanesulfonyl) imide ($LiN(CF_3SO_2)_2$, LiTFSI) and 1 mol $L^{-1}$ $LiBF_4$ in EC + GBL (1:1 by volume). $LiBF_4$ is known to have a much better thermal stability than $LiPF_6$ [40]. In particular, the stability of the $LiBF_4$ in EC/GBL electrolyte already insured the very low swelling under the high temperature storage, and the excellent safety performance against $LiCoO_2$ cathode material [41], and very good results were also obtained against LFP cathode as well [42]. Also, it has been recognized that electrolytes containing GBL are promising because this solvent has a high flame point, a high boiling point, a low vapor pressure, and a high conductivity at low temperatures [43]. Earlier works also motivates the alternative choice of LiTFSI instead of $LiBF_4$. The conductivity of the LiTFSI-based electrolyte is about $8 \times 10^{-3}$ S $cm^{-1}$ [44] using EC + GB (1:3), and its molecular weight is only 197 g. In case the anode is graphite, $LiBF_4$ is preferred to LiTFSI because it is the only salt that permits full charge–discharge cycles in GBL–EC mixtures [45]. Remember, however, that we have chosen for the anode LTO because graphite suffers at high C-rates, so that we do not have this inconvenience, here. Also, LiTFSI is known for its corrosive effect on the collector that is in aluminum [46–50], at contrast with $LiPF_6$ and $LiBF_4$ that protect the collector owing to the formation of an $AlF_3$ film [51–53], LiPF6 react with water (pmm) to form HF. However, this corrosive effect of LiTFSI occurs at 4 V and beyond, and the operating voltage with the LFP//LTO is smaller. That is why we took this opportunity to use this salt here. The diffusion coefficients of $Li^+$ ions of each component of both the LiTFSI- and the $LiBF_4$-based electrolytes considered in the present work have been determined [54], showing that they are promising for use in high-power Li-ion batteries.

For all the cells investigated in the present work, the water soluble elastomer was used as the binder for both the LFP and the LTO electrode materials. The flexibility of the electrodes is increased by a factor two with respect to the same electrodes with the conventional poly(vinylidene) fluoride (PvdF) binder [55], resulting in an improved performance at high C-rates.

## 2. Experimental

The $LiFePO_4$ sample was prepared by the hydrothermal process, particularly successful with respect to controlling the chemical composition and crystallite size [54,56–59]. We followed the procedure described in [60]. Equimolar amounts of $FeSO_4$ and $H_3PO_4$ were mixed in deoxygenated and de-ionized water. A small

amount of citric acid was added to the mixture to prevent iron oxidation. A 0.19 mol $L^{-1}$ LiOH solution was added slowly to give Fe:P:Li equal to 1:1:3. After stirring under nitrogen for about 5 min, the reaction mixture was transferred to a Parr reactor, which was purged with nitrogen and held at 220 °C for 5 h. This temperature is high enough to avoid the presence of iron on lithium site, a defect that poisons the material, when the synthesis temperature is lower the 180 °C [61]. On cooling to room temperature, the precipitate was filtered and thoroughly washed with de-ionized water. Then, it was dried at 85 °C for 24 h in a special glove box using vacuum-nitrogen scan.

The carbon coating was achieved using the procedure described elsewhere [62]. The particles were mixed with the carbon precursor (lactose) in acetone solution. The nominal dry additive corresponded to 5 wt.% carbon in $LiFePO_4$. After drying, the blend was heated at 650 °C for 2 h in an inert atmosphere to form C–$LiFePO_4$. The final quantity of carbon was about 2 wt.% of the material as measured by a carbon analyzer (CS 444, LECO Co.). This process leads to a homogeneous, 3 nm-thick surface layer of conductive carbon [63].

The C–$Li_4Ti_5O_{12}$ particles were prepared as follows. The starting materials, $TiO_2$ anatase and $Li_2CO_3$ were commercially available with purities of 99 and 99.5%, respectively. A mixture of $TiO_2$ and $Li_2CO_3$ (molar ratio Li/Ti of 2.27) was prepared, to which carbon was added under the form of 3 wt.% vapor grown carbon fiber (VGC), plus 3 wt.% Denka Black, Japan. The homogeneity of the mixture was obtained by high-energy ball milling. These precursors were mixed by jar milling in the presence of acetone used as liquid solvent. Then, the mixed powder was separated from the solvent by filtering, and dried at 120 °C for 24 h. Then the lactose was added to the product, and the same procedure as used for the carbon coating of $LiFePO_4$ was followed. The only difference is that the powder has been heated at 800 °C in $N_2$ during 12 h to form the final C–$Li_4Ti_5O_{12}$ product, instead of 650 °C in the case of $LiFePO_4$. The reason is that the conductivity of the carbon coat increases with the temperature at which it is deposited on the particles [63–65]. In the case of $LiFePO_4$, we were limited by the fact that above 700 °C, impurities are formed [66]. On the other hand, it is possible to sinter $Li_4Ti_5O_{12}$ without damaging the material and we took this opportunity to increase the conductivity of the carbon coat.

Structural analyses of the $LiFePO_4$ and $Li_4Ti_5O_{12}$ were achieved with X-ray diffraction (XRD) on a Philips X'Pert PRO MRD (PW3050) diffractometer equipped with a Cu anticathode (CuK$\alpha$ radiation $\lambda$ = 1.54056 Å) and a Bruker AXS D8 ADVANCE with Bragg–Brentano geometry, which has a sealed Co K$\alpha$ radiation source (including both K$\alpha$1 and K$\alpha$2) and linear 1-D position sensitive detector (Vantec-1), where K$\beta$ radiation is filtered by Fe foil. XRD measurements were collected in the $2\theta$ range 10–80° in step scanning mode $\Delta(2\theta)$ = 0.05°. For morphological analysis, a scanning electron microscope (SEM) study of the samples was performed using a Hitachi model HD-2700 with 200 kV, 120 kV and 80 kV operating potential. The TEM samples were ultrasonically treated in a solution of isopropyl alcohol and then deposited on silica substrate.

The electrochemical properties have been studied on cell in which the positive electrode contained 89% $LiFePO_4$ coated with carbon as active cathode material, 3% vapor grown carbon fiber, 3% carbon acetylene black (CAB) and 5% binder (SBR + CMC). The typical electrode mass and thickness of laboratory coin cell was in the range 4–8 mg and 0.02–0.06 mm, respectively The electrodes were dried at 120 °C under a vacuum and then transferred to an argon-filled glove box. The coin cells were 20 mm in diameter and 3.2 mm thick (2032 coin cells). A Celgard (3501) surfactant coated porous polypropylene separator was also used within the stainless steel case to fabricate 2032 size coin cells assembled in an argon-filled glove box. Measurements are also reported on a pilot 18650-type C–$LiFePO_4$//C–$Li_4Ti_5O_{12}$ cell. All the cells have been prepared by cycling galvanostatically first time at C/12 rate, second time at C/8, third time at C/4 at constant temperature of 25 °C. The measurements have been made using a Bitrode MCV4-100-12 cycler (maximum potential 5 V, maximum current 100 A).

The infrared camera used to determine the temperature profiles through the 18650-type cell is a Fluke Corp. camera, model Ti55, equipped with a lens of 20 mm focal length and aperture of f/0.8, operating in the wavelength range 8–14 μm.

## 3. Results

### 3.1. Structural properties

The C–$LiFePO_4$ samples have been characterized by following the quality control described in [5]. The X-ray diffraction pattern, magnetic properties and infrared spectroscopy spectrum show that the sample used in the present work are well crystallized. Since the intrinsic properties of this material are well known, and reported in different places (for a review, see [67]), they are not reported here. Fig. 1 shows the SEM images of the $LiFePO_4$ powder, showing that the average size of the particles is 90 nm. The TEM images show a uniform coat of amorphous carbon about 3 nm-thick, in agreement with the TEM images already published for this material. Fig. 2 displays the XRD pattern of the C–$Li_4Ti_5O_{12}$ composite. All of the observed diffraction peaks can be indexed according to this spinel structure (JCPDS file No. 26–1198). In particular, no line associated to $TiO_2$ has been detected (anatase at $2\theta = 25°$ and rutile at $2\theta$ = 27°), which confirms the excellent crystallinity of the material since $TiO_2$ is the impurity most frequently met in $Li_4Ti_5O_{12}$ [68]. The SEM images are presented in Fig. 3. In the figure we can see that the sample displays particles with the same size (90 nm) as the $LiFePO_4$ particles in Fig. 1. The TEM image (Fig. 4) shows the carbon layer of the C–$Li_4Ti_5O_{12}$ composite. The carbon layer covers uniformly the particles, but the surface is less regular than in the case of C–$LiFePO_4$ and varies from 1.5 to 3 nm, while it is 3 nm in $LiFePO_4$ [62].

### 3.2. Electrochemical properties

#### 3.2.1. Half-cells with $LiPF_6$ +EC + DEC in atmosphere at 25 °C

Both C-LFP and C-LTO electrodes have been tested in the usual electrolyte $LiPF_6$ in EC-DEC at low C-rate, with Li foil as counter-

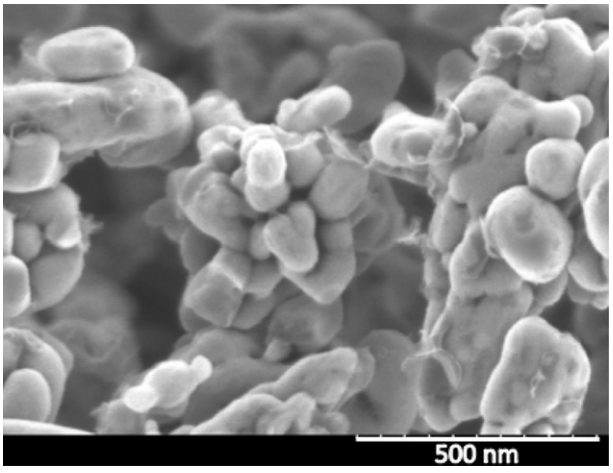


**Fig. 1.** SEM image of the C–$LiFePO_4$ composite used in this work.

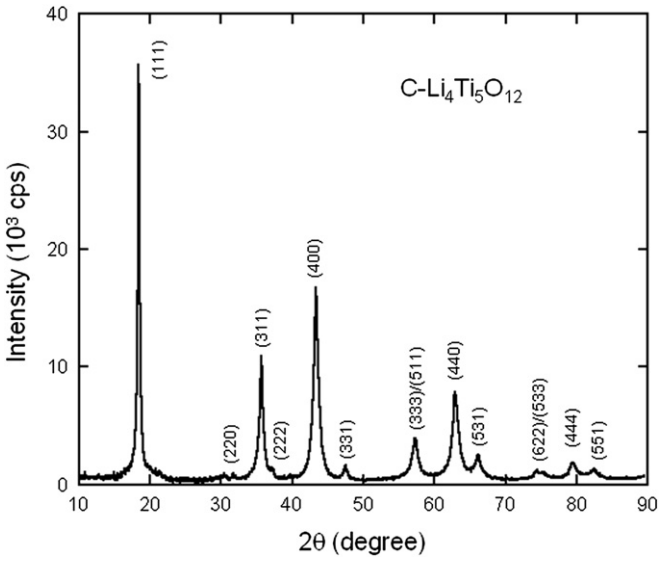


**Fig. 2.** XRD pattern of the C–$Li_4Ti_5O_{12}$ composite.

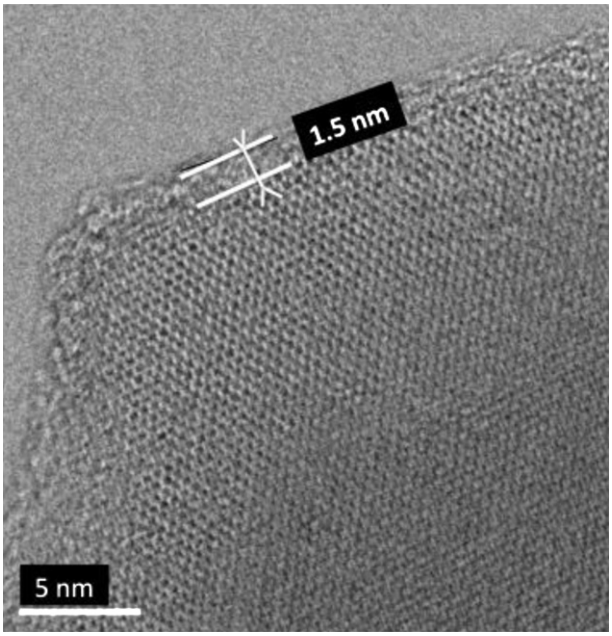


**Fig. 4.** TEM image showing the carbon layer of the C–$Li_4Ti_5O_{12}$ composite.

electrode. At C/24 rate, the voltage plateau of LFP at 3.45 V is well observed in Fig. 5, and the capacity is 154 mAh $g^{-1}$. The difference in the voltage plateau between charge and discharge does not exceed 0.05 V, which gives evidence of the small internal resistance of the cell. Another evidence of this property will be provided by the investigation of the temperature reached in the cell, investigated later on in this work. The polarization increases slowly upon increasing the C-rate, as it can be seen in Fig. 6 showing the discharge curves. The modified Peukert plot in Fig. 7 reports the discharge capacity as a function of the discharge C-rate obtained in cycles where the charge rate is C/4. It shows that the capacity is larger than 100 mAh $g^{-1}$ at 40C, which is the best performance that has been obtained so far for LFP with 90 nm-width particles.

The voltage plateau of the C-LTO/$LiPF_6$ in EC-DEC/Li cell is 1.55 V *vs.* $Li^+$/Li at low C-rate, as it can be seen in Fig. 8. These data are in agreement with prior results [67]. The voltage–capacity curves at different C-rates are shown in Fig. 9, upon charging since C-LTO is the counter-electrode. The results of the modified Peukert plot (Fig. 10) have been obtained in the voltage range 2.5–1.2 V *vs.* $Li^+$/Li. The capacity is 166 mAh $g^{-1}$ at C/24, and remains larger than 150 mAh $g^{-1}$ at 40C-rate. The comparison with Fig. 7 shows that it is larger than that of C-LFP at any rate, and that the limitation on the C-rate comes from the C-LFP side.

### 3.2.2. 18650-type cell with $LiPF_6$ + EC + DEC in atmosphere at 25 °C

The full cell has been tested in the voltage window 1.0–2.8 V upon charging and discharging, since the performance at high C-rates is important in both cases. Fast charge is convenient for use of batteries in electric transportation, fast discharge sizes the power that the battery can deliver. The discharge and charge curves of the C-LTO/$LiPF_6$ in EC-DEC/C-LFP cell are shown in Fig. 11a and b, respectively, for different C-rates. Note that in the present work, we keep the same conventional unit as in [32], namely the capacity is expressed in mAh per gram of the active negative electrode $LiFePO_4$. At low C-rate, the voltage plateau is observed at 1.85 V; this is the difference between the plateaus of the half-cells in Figs. 5

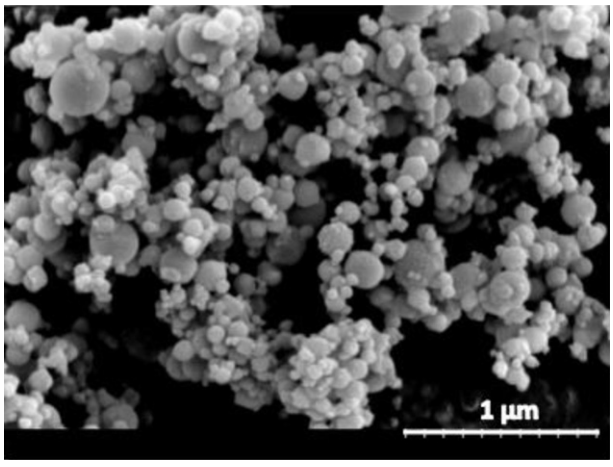


**Fig. 3.** SEM image of the C–$Li_4Ti_5O_{12}$ composite.

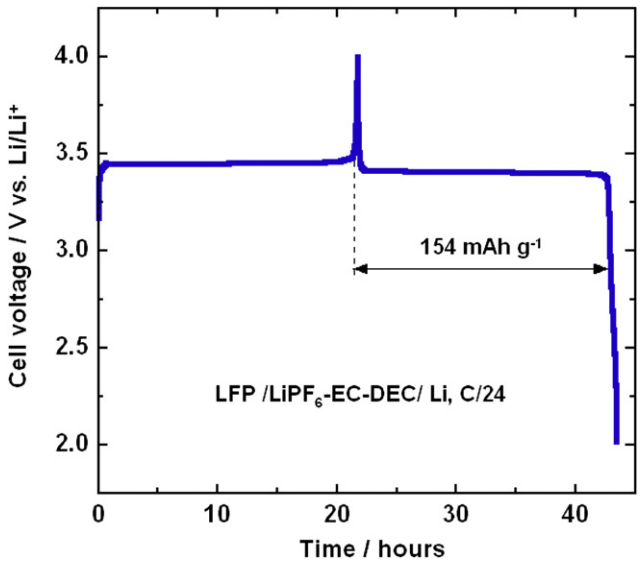


**Fig. 5.** Charge–discharge of C–$LiFePO_4$/1 mol $L^{-1}$ $LiPF_6$ in EC-DEC(1:1)/Li at C/24 rate.

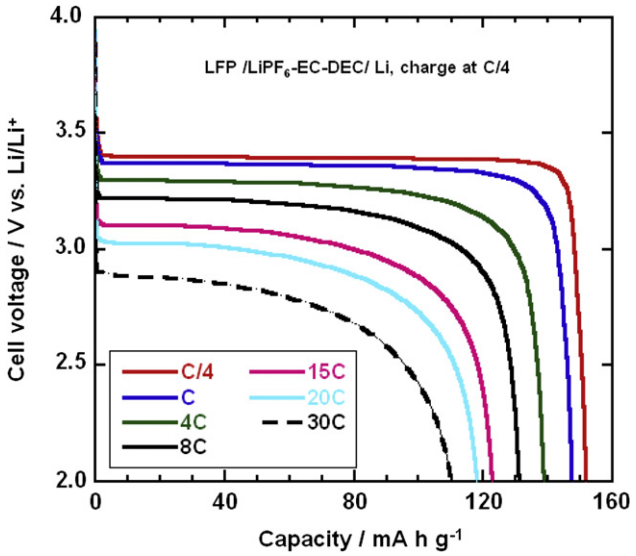


**Fig. 6.** Discharge curves of C–$LiFePO_4$/1 mol $L^{-1}$ $LiPF_6$ in EC-DEC (1:1)/Li at different C-rates.

and 8. The modified Peukert plots (measured upon discharge) and the inverse modified Peukert (measured upon charging) are reported in Fig. 12. The modified Peukert plot was measured along cycles with C/4 charge rate, as a function of the discharge rate. The inverse modified Peukert was measured along cycles with C/4 discharge rate, as a function of the charge rate. The difference upon charging and discharging is best evidenced in this last figure, and it takes place at 2C. The discharge capacity is still 80 mAh $g^{-1}$ at 40C, while the charge capacity at this rate is *ca.* 50 mAh $g^{-1}$. The discharge curves of the "18650" cell built with these materials is reported in Fig. 13, together with the modified Peukert plot. Note the performance of this "18650" cell is slightly improved with respect to the laboratory cell presented in the previous figures, at high C-rates, because it has been manufactured with the industrial optimized process. Thus, the specific energy of the 0.65 Ah 18560-type cells used in this work is 50 Wh $kg^{-1}$.

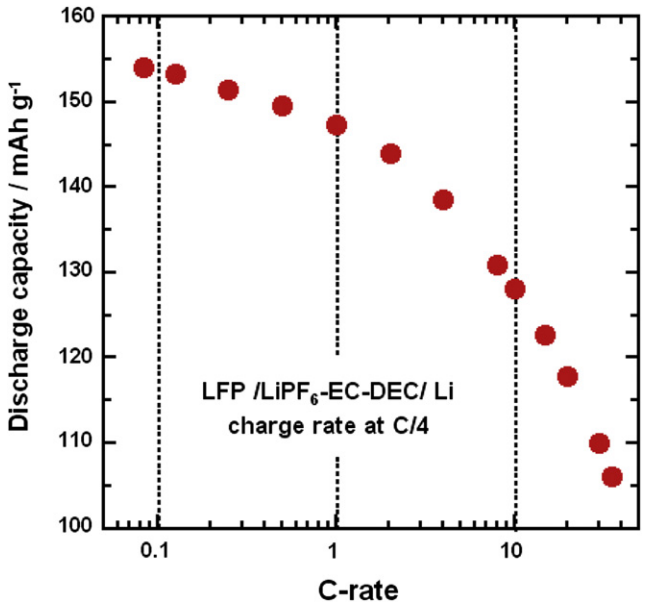


**Fig. 7.** Modified Peukert plot of the C–$LiFePO_4$/1 mol $L^{-1}$ $LiPF_6$ in EC-DEC (1:1)/Li cell.

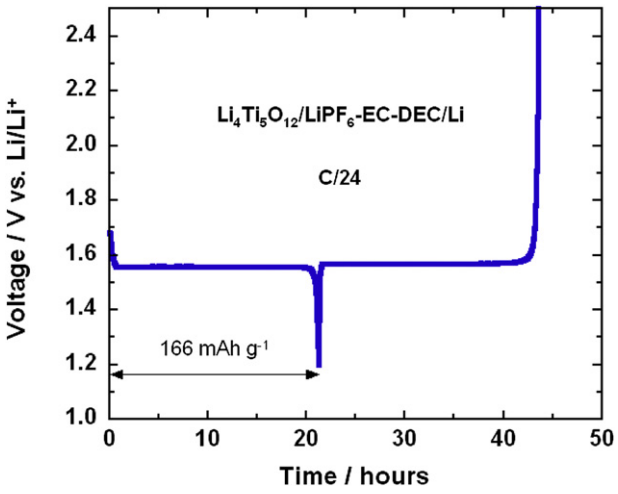


**Fig. 8.** Voltage plateau of C–$Li_4Ti_5O_{12}$/1 mol $L^{-1}$ $LiPF_6$ in EC-DEC (1:1)/Li cell at C/24 rate.

### 3.2.3. *Thermal runaway of 18650-type cell*

The study of the thermal properties of this "18650" cell is also illustrated in Fig. 14, since the temperature reached during the experiments at all steps of the modified Peukert plot is also reported. The maximum temperature reached by the cell is 34 °C at 40C-rate. This is however only an average temperature. The temperature profile of the "18650" cell has been measured under extreme charge rate conditions of 60C rate with a thermal camera. The results are reported in Fig. 15. Again, the temperature does not exceed 35 °C anywhere in the cell when the charge is limited at partial charge 1.7 V, but increases locally up to 48 °C at full charge (2.5 V). The thermal profile during the discharge at the same C-rate is shown in Fig. 16 at partial discharge 1.2 V and full discharge 1 V. Again the temperature is smaller than 40 °C anywhere inside the cell. The stability upon cycling has been tested in a protocol, where each cycle consists of float charging at 2.5 V during 5 min followed by a discharge at 5C rate. The results are reported as a function of the C-rate (charge state) the discharge in constant rate (5C). As a result, the cell remains stable over the 3500 cycles that have been tested at 30 °C (2 min), 60 °C (1 min) and 100 °C (35 s), as it can be seen in Fig. 17, which confirms our previous result according to which C-LFP//C-LTO cell does not age upon cycling [32]. At 60C

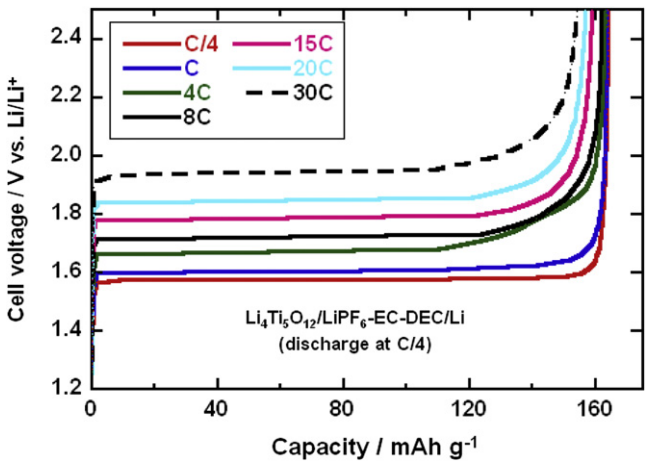


**Fig. 9.** Charge curves of C–$Li_4Ti_5O_{12}$/1 mol $L^{-1}$ $LiPF_6$ in EC-DEC (1:1)/Li at different C-rates.

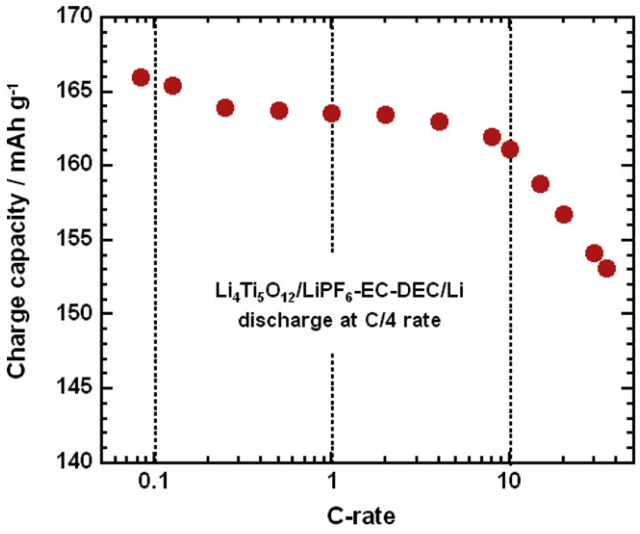


**Fig. 10.** Modified Peukert plot of the C–$Li_4Ti_5O_{12}$/1 mol $L^{-1}$ $LiPF_6$ in EC-DEC(1:1)/Li cell.

(1 min) charge rate, the capacity of the 18650 has 80% of the nominal capacity (650 mAh). This data are attractive for fast charge application such electric, bus streetcar and grid frequency regulation.

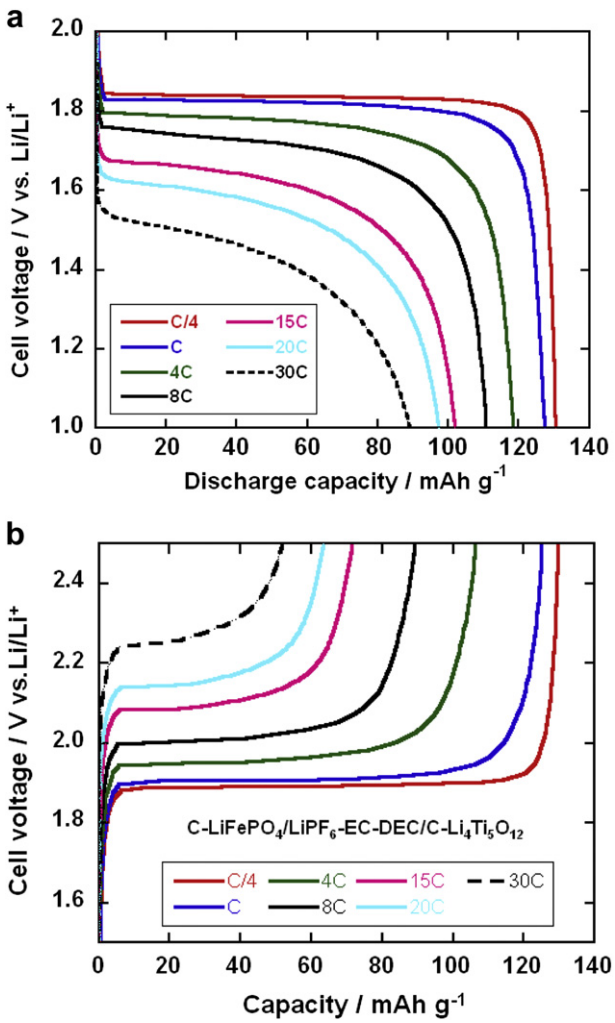


**Fig. 11.** Discharge (a) and charge (b) curves of the C–$LiFePO_4$/1 mol $L^{-1}$ $LiPF_6$ in EC-DEC (1:1)/C–$Li_4Ti_5O_{12}$ "18650" cell.

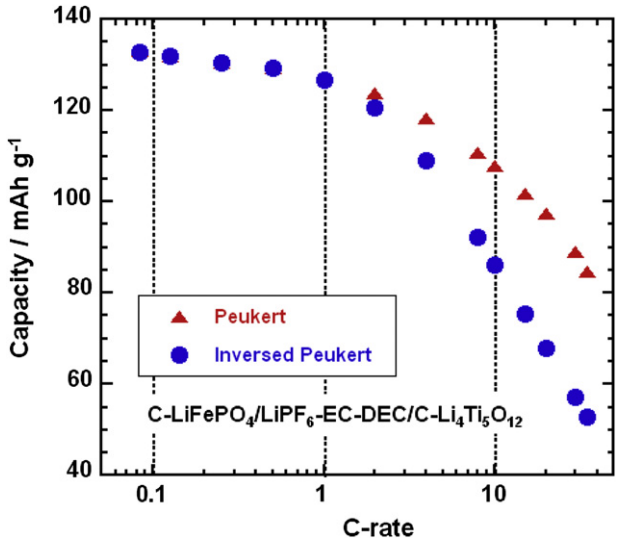


**Fig. 12.** Modified Peukert (discharge) and inverse modified Peukert (charge) plots of the C–$LiFePO_4$/1 mol $L^{-1}$ $LiPF_6$ in EC-DEC (1:1)/C–$Li_4Ti_5O_{12}$.

### 3.2.4. Coin-cells with LiTFSI in other electrolytes in atmosphere up to 60 °C

Since we have already pointed out that the $LiPF_6$-based electrolyte suffers above 30 °C, we have tested C-LFP//C-LTO coin cells with other electrolytes that are stable at higher temperature. The results are reported in Figs. 18 and 19. Note all these cells have been prepared at IREQ in the same conditions, so that direct comparison can be made. At 25 °C, the performance is nearly the same for the three electrolytes that have been considered. Note, however, that the $LiPF_6$ in EC-DEC electrolyte limits the capacity at high C-rates (>10C). On the other hand, at 60 °C, a major improvement has been achieved at any C-rate with the 0.5 mol $L^{-1}$ LiTFSI + 1 mol $L^{-1}$ $LiBF_4$ EC-GBL. The discharge capacity remains larger than 120 mAh $g^{-1}$ up to 10C. At 40C, the capacity remains as high as 92vmAh $g^{-1}$, while it has dropped at 20 mAh $g^{-1}$ with $LiPF_6$ in EC-DEC. This result can be attributed to the strong degradation of $LiPF_6$ above 30 °C. We also note that the 1.5 mol $L^{-1}$ $LiBF_4$ in EC-DEC is not significantly better than the $LiPF_6$-based electrolyte, but it is not worse, which is somehow surprising since the ionic conductivity of

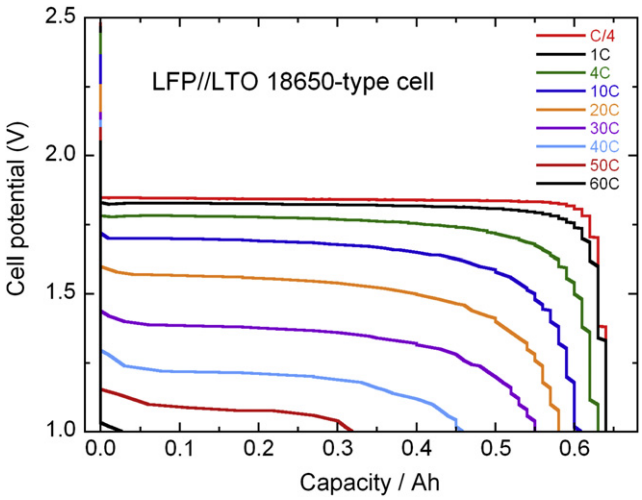


**Fig. 13.** Discharge curves of the C–$LiFePO_4$/1 mol $L^{-1}$ $LiPF_6$ in EC-DEC (1:1)/C–$Li_4Ti_5O_{12}$ "18650"-type cell at different C-rates from C/12 to 60C.

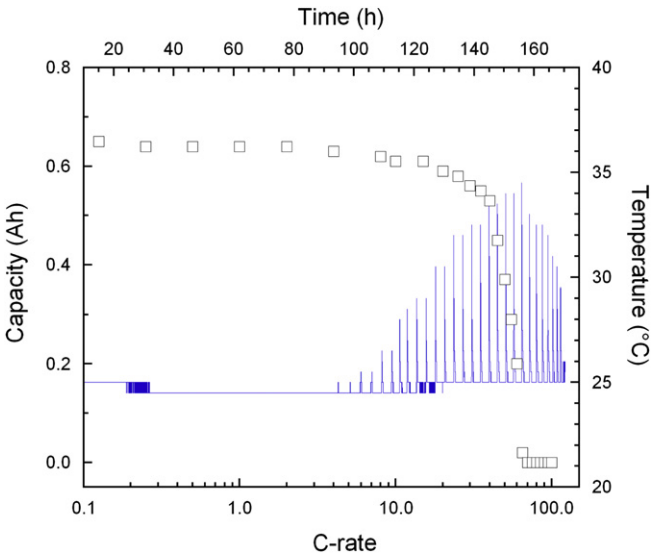


**Fig. 14.** Thermal properties of the C-LFP//C-LTO "18650"-type cell and modified Peukert plot of this cell. The average temperature of the surface of the cell (measured by thermocouple) reached at the different cycles mentioned in the modified Peukert plot is also reported (right scale).

this $LiBF_4$-based electrolyte is smaller [69]. The C–LFP/0.5 mol $L^{-1}$ LiTFSI + 1 mol $L^{-1}$ $LiBF_4$ in EC-GBL/C–$Li_4Ti_5O_{12}$ cell displays thus a major improvement as it takes benefit of the stability of LiTFSI, this battery operating remarkably at 60C rate, while the temperature even at this high rate (measured by thermocouple like in Fig. 14) is less than 50 °C.

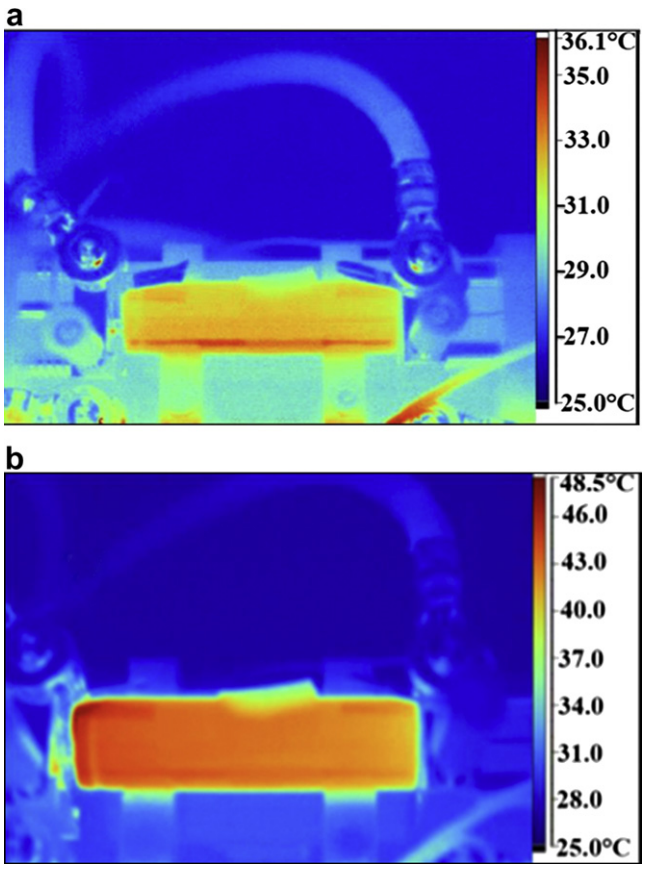


**Fig. 15.** Thermal infrared image of the LTO//LFP "18650"-type cell recorded during charge at rate 50C, at partial charge (1.7 V, upper figure) and at full charge (2.1 V, bottom). The electrolyte is with 1 mol $L^{-1}$ $LiPF_6$ in EC-DEC (1:1).

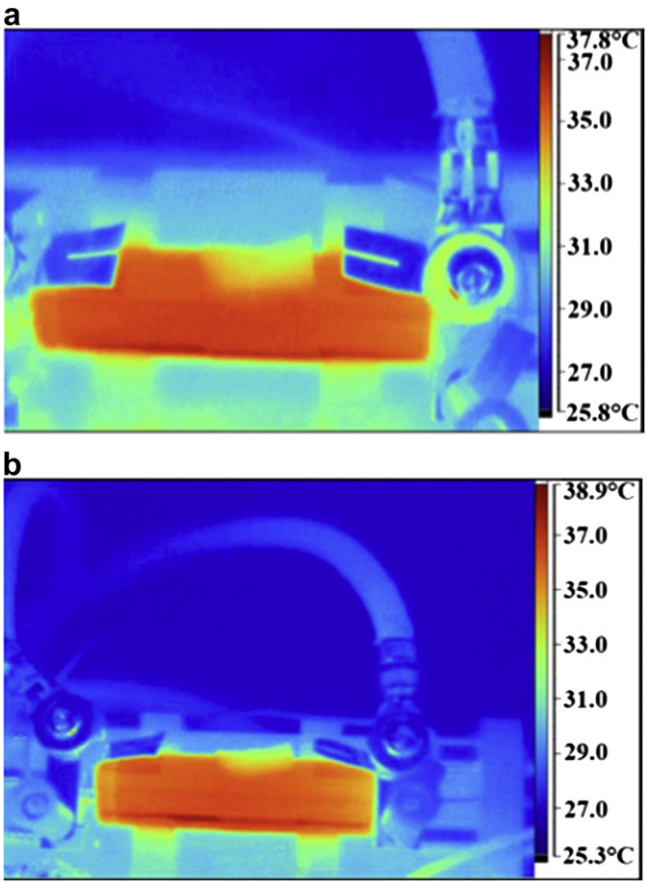


**Fig. 16.** Thermal infrared images of C-LTO//C-LFP "18650"-cell discharged at 50C rate (a) Partial discharge at 1.2 V and (b) total discharge at 1.0 V. The electrolyte is with 1 mol $L^{-1}$ $LiPF_6$ in EC-DEC (1:1).

### 3.2.5. *Coin-cells with LiFSI in other electrolytes at 80 °C*

In an attempt to rise the temperature at which a Li-ion battery can operate, we have tested another salt, namely Lithium bis(-fluorosulfonyl)imide (LiFSI). LiFSI was first claimed as conducting salt with good anticorrosive properties for Li-ion batteries in 1995 [70], but this salt is difficult to prepare with the high purity that is mandatory for its use in Li-ion batteries [71]. Now that that this problem has been overcome [72,73], this salt has a considerable interest because of its thermal behavior, stability toward hydrolysis, and ionic transport behavior [74]: it is thermally stable up to 200 °C, exhibits far superior stability toward hydrolysis than $LiPF_6$, shows a conductivity that is larger than that of LiTFSI. Moreover, the corrosive effect of LiTFSI on the Al-collector at high voltage is not observed with LiFSI, provided that the salt is pure (*i.e.* free of the $Cl^-$ impurities), at least at room temperature where the investigations have been done. In principal, this last aspect here does not directly concern us, because the operating voltage is lower owing to the choice of the $Li_4Ti_5O_{12}$ cathode, but the chemical reactions might be more severe at high temperature, and the choice of LiFSI is then more secure.

Fig. 20 shows the first cycles of C–$LiFePO_4$//C–$Li_4Ti_5O_{12}$ cell by using 1 mol $L^{-1}$ LiFSI (lithium bis(fluorosulfonyl)imide) in GBL and 1 mol $L^{-1}$ LiFSI in PC (propylene carbonate) + GBL (1:1 in volume) when the coin cells are placed in atmosphere at 80 °C. The capacity is 158 mAh $g^{-1}$ and the first coulombic efficiency (1CE) is 95%.

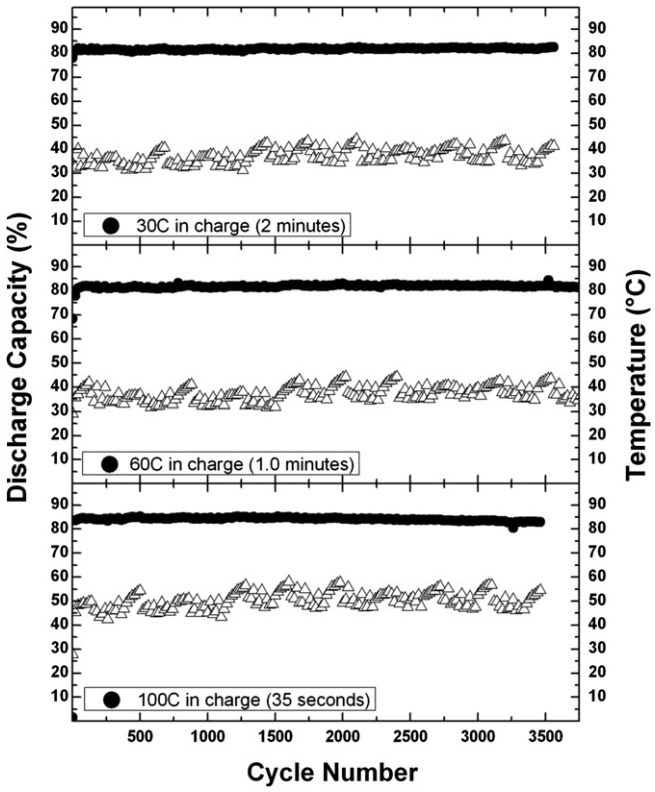


**Fig. 17.** Performance of the rapid charge rate of C-LTO//C-LFP "18650"-type cell upon cycling with 1 mol $L^{-1}$ $LiPF_6$ in EC-DEC (1:1) as electrolyte.

Addition of the PC increases both the capacity (167 mAh $g^{-1}$) and the 1 CE (99%). On another hand, with $LiPF_6$ EC + DEC and $LiBF_4$ EC + DEC electrolytes, the cells cannot be charged, because the boiling temperature of the carbonates is about the same as the temperature of the experiment.

These results at 80 °C are only preliminary because further studies of aging at this temperature on the long-term basis are still to be done before a definitive conclusion on the possibility for the Li-ion batteries C–$LiFePO_4$//C–$Li_4Ti5O_{12}$ to operate at 80 °C, but the

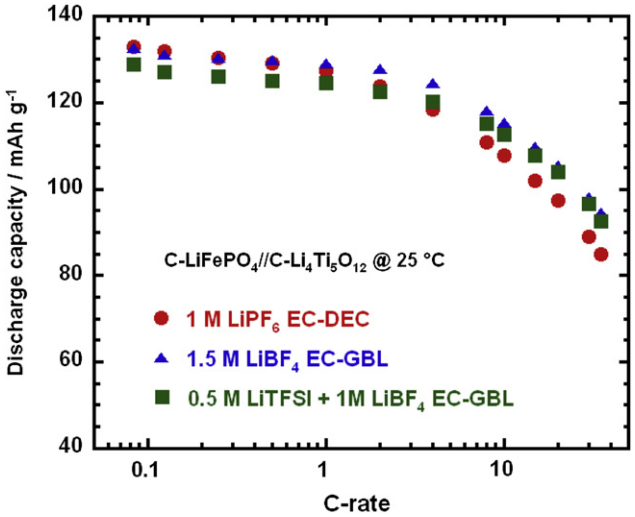


**Fig. 18.** Inverse modified Peukert at 25 °C of the C-LTO//C-LFP "18650"-type cell with different electrolytes.

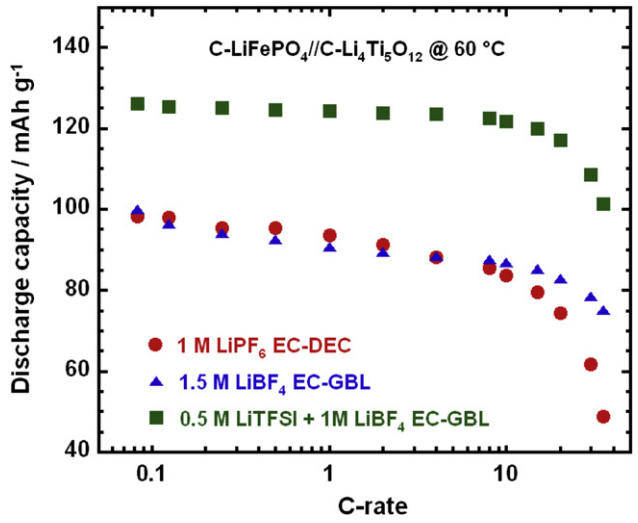


**Fig. 19.** Inverse modified Peukert at 60 °C of the C-LTO//C-LFP cell with different electrolytes.

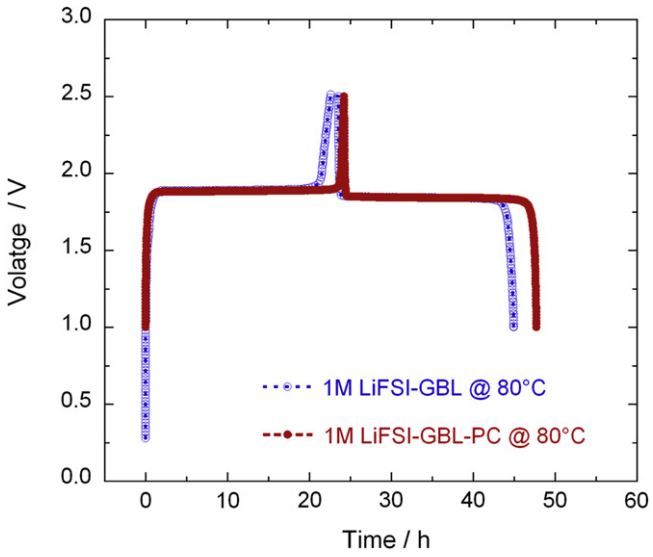


**Fig. 20.** Charge–discharge of C-LFP/LIFSI-based electolyte/C-LTO at rate C/24 at 80 °C.

results we have obtained with LiFSI in GBL are actually promising. Even at this temperature LiFSI will not generate HF, and the carbon coated LTO will suppress all the gases such $H_2$, CO, $CO_2$ ect… during charge discharge.

## 4. Concluding remarks

The Li-ion battery C–$LiFePO_4$//$Li_4Ti_5O_{12}$ has a rather small voltage of 1.88 V at low C-rate. However, it has some advantages that make it relevant to many applications as follows: (a) a lack of aging upon cycling, a property that is due to the replacement of the classical graphite anode by $Li_4Ti_5O_{12}$ and the correlated lack of solid–electrolyte interface on the anode. (b) The possibility to work at high C-rates. This is due again to the fact that $Li_4Ti_5O_{12}$ does not suffer dilatation and contraction upon lithiation or delithiation. (c) The operating voltage of $Li_4Ti_5O_{12}$ allows for the replacement of the unstable $LiPF_6$ salt that imposed the thermo-regulation of the battery at 30 °C to avoid fast degradation. We have found that the

use of LiTFSI in $LiBF_4$-based electrolyte make the battery operating nicely at 60 °C.

Of course, the power that can be delivered depends on the size of the particles. In the present work, all the tests have been made with $LiFePO_4$ and $Li_4Ti_5O_{12}$ particles that have an average size of 90 nm, which can be easily produced at the industrial scale. A "18650"-type cell built with these products has a charge capacity 0.65 Ah at low C-rate, and still 0.52 Ah at 60C (1 min). This outstanding result is primarily due to the fact that the insertion/de-insertion of Li in both the $LiFePO_4$ and the $Li_4Ti_5O_{12}$ electrodes proceeds through a two-phase reaction. It means that the nucleation rate is faster than solid-state diffusion inside the particles, and faster means more power available. However, high power also requires fast drain of the electrons to the electrodes, a result that was obtained by coating both the $LiFePO_4$ and the $Li_4Ti_5O_{12}$ particles with conductive carbon. The coating with a conductive layer is known to be mandatory since years for $LiFePO_4$. The comparison between the results in the present work, and our earlier work on LFP// LTO shows that the carbon coating of $Li_4Ti_5O_{12}$ particles also improves the power density and rapid charge, up to the point reached in the present situation where the limitation of the power is due to the positive electrode and electrolyte, rather than the negative one.

To conclude, the C–LFP/0.5 mol $L^{-1}$ LiTFSI + 1 mol $L^{-1}$ $LiBF_4$ in EC-GBL/C–$Li_4Ti_5O_{12}$ realizes a cell that can operate at least up to 60 °C without aging over thousands of cycle, even at very fast C-rates of 60C. This performance has been possible because this electrolyte is compatible with both electrodes, allowing the substitution of the $LiPF_6$ salt that ages above 30 °C by the much more stable LiTFSI. This unprecedented performance makes this battery quite promising for different applications including rechargeable hybrid vehicles and regulation of the current to solve intermittence problems on smart grids. Even float charging under severe conditions is possible without thermal runaway since the temperature never exceeded 60 °C, while the use a temperature-compensated battery charger is usually needed for valve-regulated batteries.

## References


[1] T. Yoshida, K. Kitoh, S. Ohtsubo, W. Shinoya, H. Katsukawa, J. Yamaki, Electrochem. Solid-State Lett. 10 (2007) A60.
[2] W. Lu, I. Belharouak, S.H. Park, Y.K. Sun, K. Amine, Electrochim. Acta 52 (2007) 5837.
[3] A.K. Padhi, K.S. Nanjundaswamy, J.B. Goodenough, J. Electrochem. Soc. 144 (1997) 1188.
[4] N. Ravet, Y. Chouinard, J.F. Magnan, S. Besner, M. Gauthier, M. Armand, J. Power Sources 97-98 (2001) 503.
[5] K. Zaghib, A. Mauger, C.M. Julien, J. Solid State Electrochem 16 (2012) 835.
[6] E. Ferg, R.J. Gummow, A. de Kock, M.M. Tackeray, J. Electrochem. Soc. 141 (1994) L147.
[7] T. Ohzuku, A. Ueda, N. Yamamoto, J. Electrochem. Soc. 142 (1995) 1431.
[8] K. Zaghib, M. Armand, M. Gauthier, in: J. Broadhead, B. Scrosati (Eds.), Proceeding of the Symposium on Lithium Polymer Batteries, The Electrochemical Society, Pennington, NJ, 1997, pp. 250–264.
[9] K. Zaghib, M. Armand, M. Gauthier, J. Electrochem. Soc. 145 (1998) 3135.
[10] S. Sarciaux, L.S. Sylvere, A. La Salle, D. Guyomard, Mol. Cryst. Liq. Cryst. 311 (1998) 63.
[11] S.I. Pyun, S.W. Kim, H.C. Shin, J. Power Sources 81–82 (1999) 248.
[12] A.N. Jansen, A.J. Kahaian, K.D. Kepler, P.A. Nelson, K. Amine, D.W. Dees, D.R. Vissers, M.M. Thackeray, J. Power Sources 81–82 (1999) 902.
[13] K. Zaghib, M. Simoneau, M. Armand, M. Gauthier, J. Power Sources 81–82 (1999) 300.
[14] S. Bach, J.P. Pereira-Ramos, N. Baffier, J. Power Sources 81–82 (1999) 273.
[15] P.P. Prosini, R. Mancini, L. Petrucci, V. Contini, P. Villano, Solid State Ionics 144 (2001) 185.
[16] T. Doi, Y. Iriyama, T. Abe, Z. Ogumi, Chem. Mater. 17 (2005) 1580.
[17] A. Guerfi, S. Sevigny, M. Lagacé, P. Hovington, K. Kinoshita, K. Zaghib, J. Power Sources 119 (2003) 88.
[18] L. Cheng, H.-J. Liu, J.-J. Zhang, H.-M. Xiong, Y.-Y. Xia, J. Electrochem. Soc. 153 (2006) A1472.
[19] Y. Abe, E. Matsui, M. Senna, J. Phys. Chem. Solids 68 (2010) 285.
[20] K. Mukai, K. Ariyoshi, T. Ohzuku, J. Power Sources 146 (2005) 213.
[21] C.H. Chen, J.T. Vaughey, A.N. Jansen, D.W. Dees, A.J. Kahaian, T. Goacher, M.M. Thackeray, J. Electrochem. Soc. 148 (2001) A102.
[22] X. Li, M.Z. Qu, Z.L. Yu, J. Alloys Compd. 487 (2009) L12.
[23] S.H. Huang, Z.Y. Wen, X.J. Zhu, Z.X. Lin, J. Electrochem. Soc. 152 (2005) A186.
[24] T.F. Yi, J. Shu, Y.R. Zhu, X.D. Zhu, R.S. Zhu, A.N. Zhou, J. Power Sources 195 (2010) 285.
[25] H.L. Zhao, Y. Li, Z.M. Zhu, J. Lin, Z.H. Tian, R.L. Wang, Electrochim. Acta 53 (2008) 7079.
[26] S.H. Huang, Z.Y. Wen, J.C. Zhang, X.L. Yang, Electrochim. Acta 52 (2007) 3704.
[27] (a) S.H. Huang, Z.Y. Wen, X.J. Zhu, Z.X. Lin, J. Power Sources 165 (2007) 408; (b) L.X. Yang, L.J. Gao, J. Alloys Compd. 485 (2009) 93.
[28] J.J. Huang, Z.Y. Jiang, Electrochim. Acta 53 (2008) 7756.
[29] G.J. Wang, J. Gao, L.J. Fu, N.H. Zhao, Y.P. Wu, T. Takamura, J. Power Sources 174 (2007) 1109.
[30] L. Cheng, X.L. Li, H.J. Liu, H.M. Xiong, P.W. Zhang, Y.Y. Xia, J. Electrochem. Soc. 154 (2007) A692.
[31] J. Gao, J.R. Ying, C.Y. Jiang, C.R. Wan, J. Power Sources 166 (2007) 255.
[32] K. Zaghib, M. Dontigny, A. Guerfi, P. Charest, I. Rodrigues, A. Mauger, C.M. Julien, J. Power Sources 196 (2011) 3949.
[33] K. Zaghib, P. Charest, M. Dontigny, A. Guerfi, M. Lagacé, A. Mauger, M. Kopec, C.M. Julien, J. Power Sources 195 (2010) 8280.
[34] J.B. Goodenough, Y. Kim, Chem. Mater. 22 (2010) 587.
[35] S.E. Sloop, J.K. Pugh, S. Wang, J.B. Kerr, K. Kinoshita, Electrochem. Solid-State Lett. 4 (2001) A42.
[36] H. Yang, G.V. Zhuang, P.N. Ross, J. Power Sources 161 (2006) 573.
[37] A.D. Pasquier, F. Disma, T. Bowmer, A.S. Gozdz, G.G. Amatucci, J.M. Tarascon, J. Electrochem. Soc. 145 (1988) 472.
[38] T. Zheng, A.S. Gozdz, G.G. Amatucci, J. Electrochem. Soc. 146 (1999) 4014.
[39] Y. Matsuo, R. Kostecki, F. Mc Larnon, J. Electrochem. Soc. 148 (2001) A687.
[40] E.S. Hong, S. Okada, T. Sonoda, S. Gopukumar, J.-I. Yamaki, J. Electrochem. Soc. 151 (2004) 1836.
[41] T. Ohsaki, N. Takami, M. Kanda, M. Yamamoto, Stud. Surf. Sci. Catal. 132 (2001) 925.
[42] K. Zaghib, K. Striebel, A. Guerfi, J. Shim, M. Armand, M. Gauthier, Electrochim. Acta 50 (2004) 263.
[43] N. Takami, J. Power Sources 97-98 (2001) 677.
[44] K. Zaghib, P. Charest, A. Guerfi, J. Shim, M. Perrier, K. Striebel, J. Power Sources 146 (2005) 380.
[45] A. Chagnes, B. Carré, P. Willmann, R. Dedryvère, D. Gonbeau, D. Lemordant, J. Electrochem. Soc. 150 (2003) A1255.
[46] W.K. Behl, E.J. Plichta, J. Power Sources 72 (1998) 132.
[47] H. Sakaebe, H. Matsumoto, Electrochem. Commun. 5 (2003) 594.
[48] X. Zhang, T.M. Devine, Identity of Passive Film Formed on Aluminum in Li-ion Battery Electrolytes with LiPF6, Lawrence Berkeley National Laboratory, 2008, Retrieved from: http://escholarship.org/uc/item/1wk1m1ft.
[49] S.S. Zhang, T.R. Jow, J. Power Sources 109 (2002) 458.
[50] H. Yang, K. Kwon, T.M. Devine, J.W. Evans, J. Electrochem. Soc. 147 (2000) 4399.
[51] S. Zhang, M.S. Ding, T.R. Jow, J. Power Sources 102 (2001) 16.
[52] T. Nakajima, M. Mori, V. Gupta, Y. Ohzawa, H. Iwata, Solid State Sci. 4 (2002) 1385.
[53] J.W. Braithwaite, A. Gonzales, G. Nagasubramanian, S.J. Lucero, D.E. Peebles, J.A. Ohlhausen, W.R. Cieslak, J. Electrochem. Soc. 146 (2) (1999) 448.
[54] K. Hayamizu, Y. Aihara, S. Arai, W.S. Price, Electrochim. Acta 45 (2000) 1313.
[55] A. Guerfi, M. Kaneko, M. Petitclerc, M. Mori, K. Zaghib, J. Power Sources 163 (2007) 1047.
[56] K. Zaghib, M. Armand, 5th International Conference on Polymer Batteries and Fuel Cells, Jeju Isl. Korea (2003).
[57] J. Chen, M.S. Whittingham, Electrochem. Commun. 8 (2006) 855.
[58] S. Yang, P.Y. Zavajil, M.S. Whittingham, Electrochem. Commun. 3 (2001) 505.
[59] A.V. Murugan, T. Muraliganth, A. Manthiram, J. Electrochem. Soc. 156 (2009) A79.
[60] K. Zaghib, M. Dontigny, P. Charest, J.F. Labrecque, A. Guerfi, M. Kopec, A. Mauger, F. Gendron, C.M. Julien, J. Power Sources 185 (2008) 698.
[61] J. Chen, M.J. Vacchio, S. Wang, N. Chernova, P. Zavajil, M.S. Whittingham, Solid State Ionics 178 (2008) 1676.
[62] M.L. Trudeau, D. Laul, R. Veillette, A.M. Serventi, K. Zaghib, A. Mauger, C.M. Julien, J. Power Sources 196 (2011) 7383.
[63] M.M. Doeff, Y. Hu, F. McLarnon, R. Kostecki, Electrochem. Solid-State Lett. 6 (2003) A207.
[64] C.M. Julien, K. Zaghib, A. Mauger, M. Massot, A. Ait-Slah, M. Selmane, F. Gendron, J. Appl. Phys. 100 (2006) 63511.
[65] M. Massot, K. Zaghib, A. Mauger, F. Gendron, C.M. Julien, MRS Proc. 972 (2006) 0972-AA13-07.
[66] N. Amdouni, F. Gendron, A. Mauger, H. Zarrouk, C.M. Julien, Mater. Sci. Eng. B 129 (2006) 64.
[67] K. Zaghib, A. Mauger, J.B. Goodenough, F. Gendron, C.M. Julien, in: J. Garche (Ed.), Encyclopedia of Electrochemical Power Sources, Elsevier Science, 2009.
[68] S. Scharner, W. Weppner, P. Schmid-Beurmann, J. Electrochem. Soc. 146 (1999) 857.
[69] S. Zhang, K. Xu, T. Jow, J. Solid State Electrochem 7 (2003) 147.
[70] C. Michot, M. Armand, J.Y. Sanchez, Y. Choquette, M. Gauthier, US Patent 5916475 (1999).
[71] M. Beran, J. Prihoda, Z. Zak, M. Cernik, Polyhedron 25 (2006) 1292.
[72] M. Beran, J. Prihoda, J. Taraba, Polyhedron 29 (2010) 1292.
[73] H.-B. Han, Y.-X. Zhou, K. Liu, J. Nie, X.-J. Huang, M. Armand, Z.-B. Zhou, Chem. Lett. 39 (2010) 472.
[74] H.-B. Han, S.-S. Zhou, D.-J. Zhang, S.-W. Feng, L.-F. Li, K. Liu, W.-F. Feng, J. Nie, H. Li, X.-J. Huang, M. Armand, Z.-B. Zhu, J. Power Sources 196 (2011) 3623.